 doi:10.20944/preprints202110.0196.v1

Folic Acid Decorated β-Cyclodextrin-Based Poly(ε-Caprolactone)/Dextran Star Polymer with Disulfide Bond-Linker as Theranostic Nanoparticle for Tumor-Targeted MRI and Chemotherapy

Huikang Yang[a,1], Nianhua Wang[a,1], Ruimeng Yang[a,1], Li-Ming Zhang[b]*, Xinqing Jiang[a]*

[a]Department of Radiology, Guangzhou First People's Hospital, School of Medicine, South China University of Technology, Yuexiu District, Guangzhou, Guangdong Province, 510640, People's Republic of China

[b]School of Materials Science and Engineering, Sun Yat-sen University, Haizhu District, Guangzhou, Guangdong Province, 510275, People's Republic of China

* Correspondence:

Li-Ming Zhang

School of Materials Science and Engineering, Sun Yat-sen University, Haizhu District, Guangzhou, Guangdong Province, 510275, People's Republic of China

Tel/Fax +86 13802961338

Email: ceszhlm@mail.sysu.edu.cn

Xinqing Jiang

Department of Radiology, Guangzhou First People's Hospital, School of Medicine, South China University of Technology, Yuexiu District, Guangzhou, Guangdong Province, 510640, People's Republic of China

Tel/Fax +86 13726760788

Email: eyjiangxq@scut.edu.cn

[1] These authors contributed equally to this work.

 doi:10.20944/preprints202110.0196.v1

ABSTRACT

β-cyclodextrin-based star polymers have attracted much interest because of their unique structures and potential biomedical and biological applications. Herein, we synthesized well-defined folic acid (FA)-conjugated and disulfide bond-linked star polymer ((FA-Dex-SS)-*β*CD-$(PCL)_{14}$) acted as theranostic nanoparticles for tumor-targeted magnetic resonance imaging (MRI) and chemotherapy. Theranostic nanoparticles were obtained by loading doxorubicin (DOX) and superparamagnetic iron oxide particles (SPIO) were loaded into the star polymer nanoparticles to obtain ((FA-Dex-SS)-*β*CD-$(PCL)_{14}$@DOX/SPIO) theranostic nanoparticles. *In vitro* drug release studies showed that approximately 100% of the DOX was released from disulfide bond-linked theranostic nanoparticles within 24 h under a reducing environment in the presence of 10.0 mM GSH. DOX and SPIO could be delivered into HepG2 cells efficiently, owing to folate receptor-mediated endocytosis process of the nanoparticles and GSH triggered disulfide-bonds cleaving.Moreover, (FA-Dex-SS)-*β*CD-$(PCL)_{14}$@DOX/SPIO showed strong MRI contrast enhancement properties. In conclusion, folate-decorated reduction-sensitive star polymeric nanoparticles are a potential theranostic nanoparticle candidate for tumor-targeted MRI and chemotherapy.

Keywords: star polymer, *β*-cyclodextrin, tumor-targeted, disulfide bond, theranostic nanoparticles

1. Introduction

Recently, polymeric nanoparticles have received great attention as theranostic nanoparticles with the ability to deliver drugs and contrasting agents to tumor tissue[1-4]. Doxorubicin (DOX) is widely used in clinical practice, but it still has some drawbacks that need to be overcome, including poor water solubility, a short residence times in circulation, and poor biodistribution. Furthermore, these drugs can cause serious side effects including nausea, vomiting, cardiotoxicity, myelosuppression, mucositis, hair loss and systemic toxicity[5-8]. Nanoparticles were self-assembled from

Preprints (www.preprints.org) | NOT PEER-REVIEWED | Posted: 13 October 2021 doi:10.20944/preprints202110.0196.v1

amphiphilic polymers such as block, grafted and star polymers in aqueous solution, where the hydrophobic inner core of the nanoparticles can be used to encapsulate a variety of hydrophobic guest molecules[9-11]. Polymeric nanoparticles as drug cargo can not only effectively improve the water solubility and pharmacokinetics and prevent the premature burst-release of drugs, but also enhance drug tumor selectivity [12, 13]. However, drug-loaded nanoparticles remain face great challenges, such as accumulated at off-target organs and released at the tumor site inefficiently, which directly reduces the therapeutic effects.

Currently, there has been increasing interest and attention in incorporating tumor-targeting ligands and stimuli-responsive properties into different nanoparticle systems to create "smart" nanoparticles[14]. Folic acid, galactosyl, lactosyl, RGD, transferrin, hyaluronic acid and monoclonal antibodies are widely used as targeting ligands to enhance the tumor-targeting ability of nanoparticles due to their special cell interactions and recognition[9, 15-19]. Folic acid as a targeting ligand for tumor drug therapy mainly depends on the presence of the folate receptor on the surface of target cells[20]. Folate receptors (FRs) are overexpressed on many malignant tumor cells compared with the normal cells[21]. Studies have shown that both free folate and folate-decorated nanoparticles can enter cells via folate receptor-mediated endocytosis[22]. Today, folate receptors have become an ideal ligand for tumor targeting treatment and diagnosis. Shuai's group reported a folate-encoded poly(ε-caprolactone) and poly(ethylene glycol) block polymer (folate-PEG-PCL) that were synthesized for tumor-targeting delivery of doxorubicin (DOX) and SPIO[23]. Gong and co-workers reported folic acid decorated polymer vesicles loaded with SPIO and DOX simultaneously. They confirmed that the SPIO/ DOX-loaded vesicles exhibited much higher cellular uptake, moreover the *r*2 relaxivity value much higher than Feridex[24].

Slow drug release from nanoparticles at the tumor site not only compromises therapeutic efficacy but also causes cancer cells to develop multipledrug resistance (MDR). To address the above limitations, stimuli-responsive **"**smart" drug carriers, which can release drugs rapidly due to stimulated by external signals at the tumor site,

Preprints (www.preprints.org) | NOT PEER-REVIEWED | Posted: 13 October 2021 doi:10.20944/preprints202110.0196.v1

such as redox, pH, enzyme, temperature, light, magnetic force, ultrasound, or voltage signals, have attracted much interest[1, 25]. The endogenous reductive agent glutathione (GSH) is able to cleave disulfide bonds via a redox reaction, and the concentration of GSH is abundant in the cytoplasm of tumor cells[26]. Disulfide bonds are sensitive to GSH therefore, disulfide bond-linked polymers have been extensively exploited for intracellular drug release[27, 28]. Many amphiphilic block copolymers linked with disulfide bonds have been synthesized to act as nanocarriers for intracellular drug delivery and have exhibited higher therapeutic efficacy than reduction-insensitive drug-loaded nanoparticles.

Although linear polymers are widely used for drug delivery, three-dimensional star polymers have shown great potential as drug carriers due to their unique structures and molecular properties[29, 30]. Natural *β*-cyclodextrin (*β*CD), which is linked with α-1, 4-glucosidic linkages and 7 α-D-glucose units, and *β*-cyclodextrin base star polymers have played a significant role in biomedical engineering[31, 32]. Hassan and co-workers reported the synthesis of biodendrimeric *β*-cyclodextrin as drug nanocarriers by attaching *β*CD residues to the primary or secondary face of the core *β*CD via a click reaction[33, 34]. Seven poly(ester) dendrons were selectively attached to the primary face of *β*CD via click chemistry, and the product as a drug carrier greatly improved the water solubility of albendazole [35]. Shen and co-workers prepared cyclodextrin-centred drug-conjugated amphiphilic star copolymers via the combination of controlled ring-opening polymerization and click chemistry. These drug-conjugated star copolymers showed higher drug-loading efficiency than non-drug-conjugated star copolymers[36]. *β*CD-based star polycationics, which were prepared by grafting cationic groups onto the primary or second face of *β*CD, are promising candidates for gene therapy[37, 38]. Ai and co-workers prepared an amphiphilic star polysaccharide, which through click chemistry attaching dextran to the *β*-cyclodextrin core and then modified it with aliphatic chains. After loading SPIO and DOX into the polymeric nanoparticles, the CD-Dex-g-SA/SPIO/DOX theranostic nanoparticles shown great potential for monitoring cancer cells after chemotherapy[39].

 doi:10.20944/preprints202110.0196.v1

In the present research, we report the *β*CD-based star amphiphilic polymers as tumor-targeting redox-sensitive theranostic nanoparticles for tumor therapy and diagnosis (Scheme 1). The star amphiphilic polymers, composed of PCL and folic acid-decorated dextran, were prepared via the combination of ring-opening polymerization of ε-caprolactone with a *β*CD based initiator ($(N_3)_7$-*β*CD-$(OH)_{14}$) and click conjugation with disulfide bond-linked alkyne terminated dextran (alkyne-SS-dextran) coupled with folic acid. The folic acid groups were expected to upgrade the capacity of tumor-targeting, and the introduction of disulfide bonds was expected to accelerate drug release at the tumor sites. The chemical structure was determined by FTIR and ^{1}H-NMR. Dynamic light scattering (DLS), transmission electron microscopy (TEM) and fluorescence spectral were applied to study the self-assembly behaviour of the *β*CD-based star polymer in aqueous solution. Hydrophobic DOX and SPIO were encapsulated into the hydrophobic inner core by simple dialysis technique of the nanoparticles. *In vitro* drug release was carried out in 10 mM GSH to evaluate the effectiveness of the disulfide bonds in controlled drug release. Cellular uptake of the theranostic nanoparticles was studied in the HepG2 cell line (HepG2) by using confocal laser scanning microscopy (CLSM), flow cytometry and Prussian blue staining. In comparison with counterparts, Cell apoptosis and cytotoxicity assays demonstrated that cancer cell growth was inhibited markedly by the tumor-targeting redox-sensitive theranostic nanoparticles. Furthermore, the theranostic nanoparticles showed an excellent MR T_2 contrast enhancement ability.

Preprints (www.preprints.org) | NOT PEER-REVIEWED | Posted: 13 October 2021 doi:10.20944/preprints202110.0196.v1

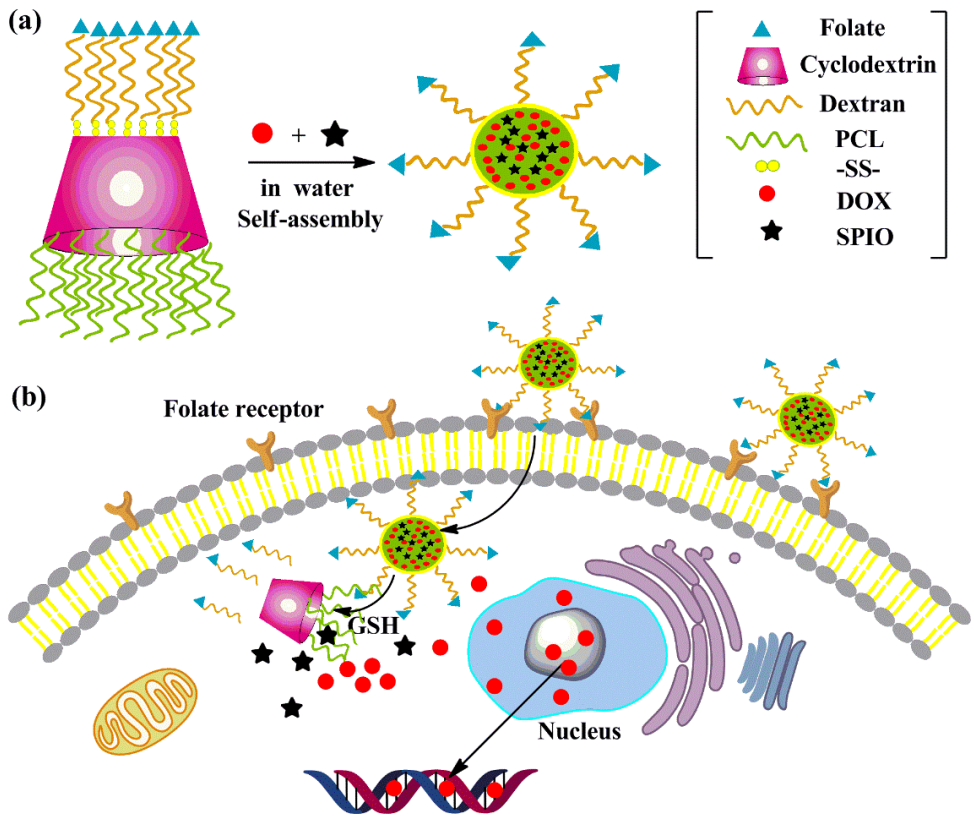

Scheme 1. (a) Schematic representation of the formation of theranostic nanoparticles, (b) Folate receptor-mediated cellular uptake and intracellular reduction controlled drug release for cancer therapy.

2. Materials and methods

2.1. Materials

Folic acid (FA, 99%), tin(II) 2-ethylhexanoate ($Sn(Oct)_2$, 95%), ε-caprolactone (ε-CL), N,N,N',N'',N''-pentamethyldiethylenetriamine (PMDTA), cuprous bromide (CuBr, 99%) were obtained from Alfa Aesar. *β*CD was purchased from Tokyo Chemical Industry Co. Ltd. (Tokyo, Japan) and recrystallized twice from water, and dried under vacuum drying oven at 50 ℃ for 2 days. Doxorubicin hydrochloride (DOX.HCl), sodium cyanoborohydride ($NaBH_3CN$, 98%), iodine (I_2, 98%), triphenylphosphine (TPP, 98%) and glutathione (GSH) were acquired from Aladdin Chemical Company. Sodium azide (NaN_3, 99%). Dextran (Mn=6600 g/mol), propargylamine (98%) and cystamine dihydrochloride (98%) were acquired from Sigma-Aldrich. Hydroxybenzotriazole (HOBT, 99%) and N-ethyl-N'-(3-dimethylaminopropyl)

Preprints (www.preprints.org) | NOT PEER-REVIEWED | Posted: 13 October 2021 doi:10.20944/preprints202110.0196.v1

carbodiimide hydrochloride (EDCI, 98%) were purchased from J&K Chemical Reagent Inc. Dulbecco's modified Eagle medium (DMEM), trypsin-ethylenediaminetetraacetic acid (trypsin-EDTA) and fetal bovine serum (FBS) were purchased from Gibco-BRL (Canada). 4′6-Diamidino-2-phenylindole (DAPI) was purchased from Beyotime Institute of Biotechnology (China). 3-(4, 5-Dimethylthiazol-2-yl)-2, 5-diphenyltetrazolium bromide (MTT) was purchased from Invitrogen Corporation (Washington, USA). All other reagents were of analytical grade and used without further purification. The human hepatocellular liver carcinoma (HepG2) cell line was purchased from the Animal Center of Sun Yat-sen University (Guangzhou, China). DMSO-*d*6 and $CDCl_3$ used as solvents in the NMR measurements were purchased from Aldrich. All other reagents were used as received without further purification.

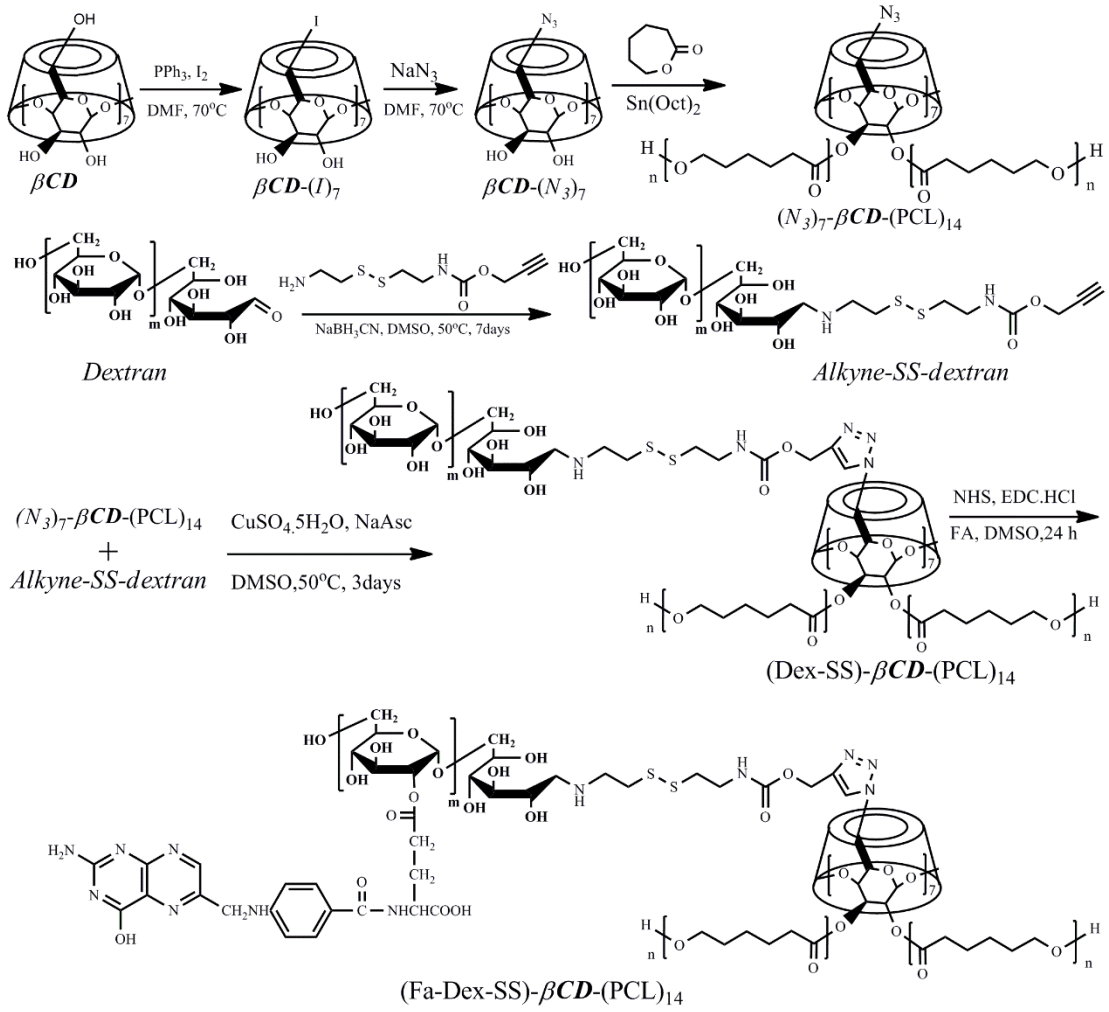

Scheme 2. Synthetic route of Folic acid decorated *β*-cyclodextrin-based poly(ε-caprolactone)/dextran star polymer.

Preprints (www.preprints.org) | NOT PEER-REVIEWED | Posted: 13 October 2021 doi:10.20944/preprints202110.0196.v1

2.2 Synthesis of heptakis(6-deoxy-6-azido)-*β*-cyclodextrin centered 14-arm star poly(ε-caprolactone)s ($(N_3)_7$-*β*CD-$(PCL)_{14}$) via ring-opening polymerization

To obtain the targeted product $(N_3)_7$-*β*CD-$(PCL)_{14}$ via the ring-opening polymerization of ε-CL when existing $Sn(Oct)_2$, the multifunctional initiator heptakis(6-deoxy-6-azido)-*β*-cyclodextrin was first prepared as Liu et al reported [40]. Typically, 18.36 g of Ph_3P (70 mmol) was dissolved in anhydrous DMF, then 17.77 g of I_2 (70 mmol) was added in 10 minutes. The Schlenk flask was placed in an oil bath regulated at 70 °C under static nitrogen pressure. Dry *β*-cyclodextrin (5.68 g, 5 mmol) from a vacuum oven was weighed in a glovebox and added to the mixture solution. The black solution was stirred for 24h at 70 °C under a N_2 atmosphere. Next, approximately 70 mL of the organic solvent DMF was removed under vacuum. The obtained residue was placed in an ice-water bath, then added 30 mL of sodium methoxide (3.0 M in methanol) under stirring. The organic solution was removed under vacuum distillation to acquire black solid residues. The obtained residue was repeatedly refluxed with a Soxhlet extractor, using methanol as the medium for 24 h. After that, the white product heptakis(6-deoxy-6-iodo)-*β*-cyclodextrin ($(I_2)_7$-*β*CD) was collected and dried 24h under vacuum at 35 °C . A total of 2.31 g of $(I_2)_7$-*β*CD (1.3 mmol) was weighed and introduced in a Schlenk flask containing 25 mL of anhydrous DMF, and then added 1.01 g NaN_3 (15 mmol). The solution was stirred continuously for 2 days at 70 °C. The organic solvent was removed under reduced pressure and white solid was collected after filtration when the reaction was accomplished. The solid was dried under vacuum at 35 °C for 1 day after being washed with cool water.

A typical synthetic procedure for *β*-cyclodextrin centred 14-arm star poly(ε-caprolactone)s ($(N_3)_7$-*β*CD-$(PCL)_{14}$) was as follows. First, 0.057 g of $(N_3)_7$-*β*CD (0.6 mmol of OH group), 1.71 g of ε-CL (15 mmol), 0.1 mL of $Sn(Oct)_2$ (0.1 mol/L in toluene) and dry toluene (5.0 mL) were added to the flame-dried Schlenk flask with a magnetic stirrer. After the toluene solution and water were removed entirely under

Preprints (www.preprints.org) | NOT PEER-REVIEWED | Posted: 13 October 2021 doi:10.20944/preprints202110.0196.v1

vacuum, the argon was exchanged three times with air. The product was vigorously stirred for 24h in 110°C oil bath, the reaction was quenched rapidly by cooling to ambient temperature, and THF was added to the Schlenk flask to dissolve the crude product. Then, the mixture solution was transferred into excessive petroleum ether to collect the sediments and under vacuum for 24 h until constant weight was reached (1.67 g, 94.5% overall yield, *M*n =42300, *M*w/*M*n = 1.17). ^{1}H NMR analysis revealed the degree of polymerization (DP) for the PCL-OH segments was 23. ^{1}H NMR of PCL (500.10 MHz, $CDCl_3$, 298 K), δ, ppm): 4.1-3.8 (-COOCH_2CH_2-), 3.6 (-CH_2CH_2OH), 2.4-2.2 (-CH_2CH_2COO-) and 1.17-1.12 (-COOCH$_2$CH_2CH_2CH_2CH$_2$-). FTIR (cm^{-1}): 1727, 1601, 1489, 1453.

2.3 Preparation of disulfide-containing α-alkyne dextran (alkyne-SS-Dex) by reductive amination

As Scheme 1 depicted, the disulfide bonds and the alkyne group were introduced to the dextran end of the molecule simultaneously through reductive amination[41]. Experimentally, 1.2 g of dextran (0.2 mmoL) and propargyl carbamate ethyl dithio ethylamine (PPA-Cyst) were dissolved in DMSO (20 mL), and 0.64 g of $NaBH_3CN$ was added to the mixture solution as a reducing agent when continuous stirring. 20 mg $NaCNBH_3$ was given every day to sustain the reductive amination at 50°C for one week. Subsequently, the mixture was transferred into a dialyzed tube (MWCO 1000 Da) and dialysis against acetate buffer (pH=5.6) for 24 h and deionized water for 48 h. The dialysate was lyophilized to acquire white powder (1.1 g, 87%).

2.4 Synthesis of star polymer (Dex-SS)$_n$-βCD-(PCL)$_{14}$ by click reaction

Click conjugations between alkyne and azido groups are widely used to prepare star polymers[34, 42]. Herein, via a click conjugation method between alkyne-SS-Dex and ((N$_3$)$_7$-βCD-(PCL)$_{14}$) to obtain the star polymer (Dex-SS)$_n$-βCD-(PCL)$_{14}$ was. Briefly, 2.4 g of alkyne-SS-Dex (0.4 mmol of alkyne group) and 0.24 g of (N$_3$)$_7$-βCD-

Preprints (www.preprints.org) | NOT PEER-REVIEWED | Posted: 13 October 2021 doi:10.20944/preprints202110.0196.v1

$(PCL)_{14}$ (0.04 mmol of azido group) were added to a round-bottom flask containing 30 mL of anhydrous DMSO under an argon atmosphere, after argon continued bubbling about 15 min, PMDETA was offered. Then, the mixture solution was further bubbled with argon for 15 min after CuBr (30 mg, 0.21 mmol) was introduced. Subsequently, the flask reacted in an oil bath at 50 °C for 3 days. The crude product was transferred into a dialysis tube (MWCO 30000 Da), and the copper salt was removed by 5% disodium ethylene diate (EDTA-2NA) solution for 2 days, and the excess alkyny-SS-dex was removed by pure water for 3 days. The dialysate was lyophilized to acquire white powder (0.42 g, 87.5%).

2.5 Prepare of folic acid decorated *β*-cyclodextrin-based poly(ε-caprolactone)/dextran star polymer

Folic acid was conjugated onto the star polymer $(Dex\text{-}SS)_n$-*β*CD-$(PCL)_{14}$ via an esterification reaction between the γ-carboxylic acid group of FA and the hydroxyl group of Dex. Experimentally, 0.20 g of $(Dex\text{-}SS)_n$-*β*CD-$(PCL)_{14}$ and 0.02 g of folic acid (0.045 mmol) were weighed and dissolved together in 20 mL anhydrous DMSO, and then EDCI (0.017 g, 0.09 mmol), HOBT (0.012 g, 0.09 mmol) were added to the solution. The flask was sealed and covered with aluminium foil, and then the mixture solution stirred for 24 h under N_2 protection. The excess FA of mixture solution was removed by dialyzed against deionized water for 3 days. Finally, folic acid modified *β*-cyclodextrin-based poly(ε-caprolactone)/dextran star polymer ($(FA\text{-}Dex\text{-}SS)_n$-*β*CD-$(PCL)_{14}$) yellow powder was obtained after freeze-drying the dialysate. The degree of substitution (DS) of FA in the synthesized polymer was determined by ^{1}H-NM and calculated as follows:

$$DS_{FA}=((I_a\times441)/2)/(I_{2\text{-}6})/5\times162\times100\% \quad (1)$$

where I_a is the integral for the protons of poison ring in FA, $I_{2\text{-}6}$ is the integral for the protons of $I_{2\text{-}6}$ in dextran between 3.2 and 4.0 ppm. For comparison, FA-decorated reduction insensitive star polymer (FA-Dex)-*β*CD-$(PCL)_{14}$, reduction insensitive star polymer (Dex)-*β*CD-$(PCL)_{14}$ and FA-decorated reduction insensitive star polymer (FA-Dex)-*β*CD-$(PCL)_{14}$ with similar compositions were also prepared.

Preprints (www.preprints.org) | NOT PEER-REVIEWED | Posted: 13 October 2021 doi:10.20944/preprints202110.0196.v1

2.6 Characterization

A Perkin-Elmer Paragon1000 spectrometer, which scanning range was from 500 to 4000 cm^{-1}, was used to record the FTIR spectra by virtue of the potassium bromide (KBr) method at room temperature. The detailed chemical structure of the products was measured on a Bruker 500 NMR spectrometer by deuterated chloroform ($CDCl_3$-*d*) or deuterated dimethyl sulfoxide (DMSO-d_6, contain tetramethylsilane (TMS)) as the internal standard, respectively. The number average molecular weight (M_n) and molecular weight polydispersity index (M_w/M_n) of the βCD-$(PCL)_{14}$ were recorded by gel permeation chromatography (GPC) adopting a Waters 1515 pump and Waters 2414 differential refractive index detector. The column system was calibrated with a set of monodisperse polystyrene standards using HPLC grade THF as mobile phase with a flow rate of 0.8 mL/min at 30 °C. A Brookhaven BI-200SM Goniometer particle size analyzer (Brookhaven Instruments Corporation, USA) was used to determine the hydrodynamic diameter and size distribution of the nanoparticles. The data was a record lasting 300 s collected by an auto-correlator at 25 °C with a detection angle of scattered light at 90°. For each nanoparticle solution, the concentration was fixed at 1 mg/mL and filtered through a 0.45 μm filter. All the data was collected from three measurements. The morphology of the nanoparticles was revealed from a JEOL JEM-2100F transmission electron microscope (TEM, JEM-2100F, JEOL, Tokyo, Japan) operated at an accelerating voltage of 200 keV. A small drop of micelle solution was suspended on the copper grid surface, then the solution was blotted off with filter paper after 1 min. After that, the sample was negative stained with 1 wt% phosphotungstic acid solution (2 wt% in water) for 20 seconds, and the solution was blotted off with filter paper. The grid was completely dried before TEM observation.

2.7 Nanoparticles formation and the critical micellar concentration

Typically, 10 mg of star polymer was dissolved in 2 mL of warm DMSO, and the organic solution was added dropwise into 5 mL 5 mL vigorous stirring deionized water. After the addition of the organic solution, the micelle solution was further stirred for 1 h, and then the mixture solution was placed in a dialysis tube (molecular weight cut-off

Preprints (www.preprints.org) | NOT PEER-REVIEWED | Posted: 13 October 2021 doi:10.20944/preprints202110.0196.v1

(MWCO) 3500 Da) and dialyzed against deionized water for 48 h to remove the DMSO. The nanoparticle solution was filtered through a 0.45 μm filter and the final concentration was adjusted to 1 mg/mL.

The critical micellar concentration (CMC) of the final product was determined by the fluorescence probe technique using pyrene as a fluorescence probe[16, 43]. Aliquots of pyrene stock solution (6×10^{-5} M in acetone, 50 μL) were added to 10 mL Eppendorf tubes, and the acetone was evaporated under vacuum. Then, polymer solutions at different concentrations were added to the Eppendorf tubes, for a final concentration of pyrene of 6×10^{-7} M in water. The combined solutions of pyrene and polymer were kept on a shaker at 37 °C for 24 h in the dark to reach the solubilization equilibrium before measurement. The fluorescence excitation spectra were obtained on a Shimadzu RF-5301PC fluorescence spectrometer at an emission wavelength of 373 nm and 5 nm bandwidth, and the scanned range was from 300 to 350 nm at room temperature.

2.8 Preparation of DOX and SPIO co-loaded nanoparticles

Ten milligrams of star polymer, 2.0 mg of DOX.HCl and an equimolar amount of triethylamine (TEA) were co-dissolved in 2 mL of warm DMSO, and then the organic solution was added dropwise to 5 mL of deionized water with vigorous stirring to load the hydrophobic DOX into the inner core of the nanoparticles. The mixture solution was further stirred for 1 h, placed in a dialysis tube (MWCO 3500 Da) and dialyzed against deionized water for 48 h to remove excess DMSO and unloaded DOX. Hydrophobic SPIO (1.5 mg) was dissolved in 1 mL trichloromethane, and then the organic solution was slowly added into the DOX-loaded nanoparticle solution under sonication. The trichloromethane was removed from the mixture via rotary evaporation. The obtained solution was passed through a 0.22 μm syringe filter to remove the unloaded SPIO precipitate and the final volume of the solution was adjusted to 10 mL. After dialysis, the UV absorption of the DOX/SPIO loaded nanoparticles was analysed by using a Shimadzu UV-3150 UV-vis spectrometer at λ_{max}=485 nm. Quantification was performed from the calibration curve of DOX in a water/DMSO (v/v=30:70) mixture. The DOX loading content (DLC) was calculated from the followed equation:

Preprints (www.preprints.org) | NOT PEER-REVIEWED | Posted: 13 October 2021 doi:10.20944/preprints202110.0196.v1

$DLC(\%)=w_1/w_2\times100$ (2)

where w_1 is the weight of the loaded drug and w_2 is the weight of the star polymer.

Atomic absorption spectroscopy (AAS) analysis was carried out, and the Fe concentration was determined at the specific Fe absorption wavelength (248.3 nm) based on a previously established calibration curve. The SPIO loading content (SLC) was calculated from the following equation:

$SLC(\%)=w_3/w_2\times100$ (3)

where w_3 is the weight of the loaded SPIO and w_2 is the weight of the star polymer.

2.9 *In vitro* DOX release from nanoparticles

In vitro DOX release from the drug-loaded nanoparticles was investigated in two different media (0 mM or 10 mM GSH) at 37 °C. Specifically, 3 mL of DOX loaded nanoparticle solution was sealed in a dialysis bag (MWCO 3500 Da) and transferred to 27 mL of PBS containing 0 or 10 mM GSH with gentle shaking at 100 rpm in a 37 °C water bath. At scheduled time intervals, 3 mL of the external solution was replaced with 3 mL of fresh buffered solution, DOX release was determined by UV-vis spectrometer (UV-3150, Shimadzu, Japan) at a wavelength of 485 nm [43].

$$E_r(\%) = \frac{V_e \sum_1^{n-1} C_i + V_0 C_n}{m_{DOX}} \times 100\% \quad (4)$$

where m_{DOX} represents the amount of doxorubicin in the nanoparticles, V_0 is the whole volume of the release media (V_0 =30 mL), V_e is the volume of the replace media (V_e =3 mL), and C_i represents the concentration of DOX in the *i*th sample.

2.10 Cellular internalization of Nanoparticles studies

Confocal laser scanning microscopy (CLSM) was exploited to illustrate the interaction between free DOX or DOX-loaded nanoparticles and tumor cells. HepG2 cells were seeded in a 6-well plate at a density of 1×10^6 cells/well in 2 mL of DMEM, and cultured at 37 °C in the 5% CO_2 atmosphere overnight. After the culture medium was replaced with DMEM containing free DOX or DOX/SPIO loaded nanoparticles (DOX concentration: 10 μg/mL). After 4h further incubated, the cells were rinsed with PBS two times and then fixed by 200 μL of 4% paraformaldehyde solution at room temperature for 30 min. Then the cells were rinsed with PBS three times, DAPI was

Preprints (www.preprints.org) | NOT PEER-REVIEWED | Posted: 13 October 2021 doi:10.20944/preprints202110.0196.v1

used to dyed cell nuclei for 30 min, and the free dye was washed out with PBS three times. Finally, fluorescence images were captured on a Leica TCS-SP2 confocal laser scanning microscope (Leica, Germany). The excitation wavelength for DOX was 485 nm and that for DAPI was 358 nm. Emission wavelengths were 590 nm for DOX and 455 nm for DAPI.

Flow cytometry was used to quantitatively analyze fluorescence intensity of DOX in HepG2 cells. HepG2 cells were inoculated with 1× 106 cells/well in a 6-well plate and cultured at 37 °C under 5% CO_2 atmosphere for 24 h. After removing the culture medium, the cells were incubated with free DOX or loaded DOX/SPIO nanoparticles in DMEM at a concentration of 10 μg/mL for 4 hours. , Then the cells were rinsed with PBS and treated with trypsin. Then, 2 mL of complete DMEM was added into a 6-well plate and the cells were collected and resuspended in 0.3 mL of PBS.. Cellular uptake of DOX was quantified by Guava easy Cyte 5HT-2L flow cytometer (Merck Millipore, Germany).

Prussian blue staining was performed to detect the cellular uptake of SPIO. In brief, HepG2 cells were inoculated with 1× 10^6 cells/well in a 6-well plate and cultured for 24 h at 37 °C under 5% CO_2 atmosphere, then the cells were incubated with SPIO-loaded nanoparticles for an additional 4 h. The cells were rinsed out with PBS, and the Prussian blue solution was incubated with cells for 30 min in the dark after fixed with 4% paraformaldehyde. Finally, HepG2 cells were washed with PBS, and Prussian blue-stained images were collected with an Olympus BX51 optical microscope.

2.11 Cell cytotoxicity assays

The in vitro cell cytotoxicity was evaluated on Human hepatocellular liver carcinoma cells using a standard MTT assay. HepG2 cells (1×10^4 cells/well in 100 μL of DMEM) were inoculated into a 96-well plate and incubated 24 h at 37 °C under a 5% CO_2 atmosphere. The culture medium was replaced with fresh DMEM containing different DOX concentration (0-10 μg/mL), and incubation for 24 or 48 h. After co-incubation with the cancer cells for 24 or 48 h, the previous medium was removed, then MTT solution (20 μL/well, 5 mg/mL) was added to the 96-well plate. In order to ensure

Preprints (www.preprints.org) | NOT PEER-REVIEWED | Posted: 13 October 2021 doi:10.20944/preprints202110.0196.v1

that MTT could transform into Formazan crystals, the cells were incubated at 37℃ for 4 h. After that, all the supernatants were discarded from the wells and replaced with 200 μL of DMSO, and then the plates were shaken for 10 min to dissolve the formazan crystals. Finally, the absorbance at 490 nm was detected by the microplate reader.

$$\text{Cell viability (\%)} = [A_{490}\text{ (sample)} / A_{490}\text{ (control)}] \times 100 \quad (5)$$

Where A_{490} (sample) and A_{490} (control) were illustrated the absorbances of the sample and control wells, respectively.

2.12 Cell apoptosis

The dyes calcein -AM and Propidium Iodide (PI) were exploited to label apoptotic cells and dead cells. HepG2 cells were seeded into 12-well plates (1×10^4 cells per well) and incubated overnight. Then, the cells were treated with various concentrations (2.5, 5 and 10 μg/mL DOX) free DOX or DOX/SPIO-loaded nanoparticles for 24 h. After that, the cells were collected, washed with PBS two times, and re-suspended in 200 μL of binding buffer. 5 μL of DAPI (E_X = 358nm, E_M = 455nm) solutions and 5 μL of Annexin V-fluorescein isothiocyanate (FITC) (E_X = 488nm, E_M = 530 nm) were added to incubate for 15 minutes on ice to stain dead or apoptotic cells. Finally, the cell apoptosis rates were detected by Gallios flow cytometer.

2.12 Relaxivity measurement

The T_2 relaxivity of the DOX/SPIO loaded nanoparticles was recorded on a clinical 3.0 T MRI scanner (Verio, Siemens, Erlangen, Germany) at room temperature, and followed measurement parameters used to measure the transverse relaxation time, TR: 1000 ms, TE: 13.8/27.6/41.4/55.2/69.0 ms, flip angle: 180°, slice thickness: 3.0 mm and matrix: 444 × 448. Relaxation times were obtained by fitting the multiecho data to a monoexponential decay curve using linearized least-squares optimization. Relaxivity values were calculated via linear least-squares fitting of 1/relaxation time (s^{-1}) versus the iron concentration (mM Fe).

Preprints (www.preprints.org) | NOT PEER-REVIEWED | Posted: 13 October 2021 doi:10.20944/preprints202110.0196.v1

3. Results and discussion

3.1 Preparation and characterization of folic acid decorated *β*-cyclodextrin-based poly(ε-caprolactone)/dextran star polymer

As Scheme 2 illustrates, folic acid-decorated *β*-cyclodextrin-based poly(ε-caprolactone)/dextran star polymer was synthesized by combination of ring opening polymerization (ROP), a copper(I)-catalysed azide-alkyne cycloaddition reaction, and a standard esterification reacted between dextran and folic acid when EDCI and HOBt existed. First, $(N_3)_7$-*β*CD-$(PCL)_{14}$ was obtained in two steps: (i) first, the 7 primary hydroxyl groups of *β*CD were selectively modified into azido groups ($(N_3)_7$-*β*CD-$(OH)_{14}$), and (ii) the remaining 14 secondary hydroxyl groups were used as initiators for the ROP of ε-CL in the presence of stannous octoate. The synthesized polymer $(N_3)_7$-*β*CD -$(OH)_{14}$ was characterized by ^{1}H NMR. From Figure 1(A), we found that the proton signal for 1C-H was located at 4.9 ppm, and the proton signal peaks that appeared between 3.11 to 3.82 belonged to 2C-H ~ 6C-H. The hydroxyl proton signal peaks for 2 C and 3C were located at 5.72 and 5.87 ppm, respectively, and the hydroxyl proton signal peak for 6-CH_2OH at 4.50 ppm completely disappeared, indicating the successful preparation of $(N_3)_7$-*β*CD-$(OH)_{14}$.

Then, $(N_3)_7$-*β*CD-$(OH)_{14}$ was used as a multifunctional initiator, and 14-arm $(N_3)_7$-*β*CD-$(PCL)_{14}$ was synthesized through the ring-opening polymerization of ε-CL when $Sn(Oct)_2$ existed at 110 °C overnight. Figure 1(B) showed the gel permeation chromatography (GPC) traces of the obtained $(N_3)_7$-*β*CD-$(PCL)_{14}$, and we saw a relatively sharp and symmetrical elution peak. However, the appearance of slight tailing in the low-molecular-weight region was the manifestation of chain transfer side reactions during polymerization. Similar results have been reported by Gou et al[36]. The average molecular weight was 42300 g/mol, the weight average molecular weight was 49500 g/mol, and the molecular weight distribution determined by GPC was 1.17.

The chemical structure of $(N_3)_7$-*β*CD-$(PCL)_{14}$ was further confirmed by FTIR and ^{1}H NMR. As Figure 1 (C) showed that an absorbance peak at 2110 cm^{-1} in the FTIR spectrum belonged to the azide groups, while the absorption peaks of ^{1}H NMR that

Preprints (www.preprints.org) | NOT PEER-REVIEWED | Posted: 13 October 2021 doi:10.20944/preprints202110.0196.v1

appeared at 2934 cm^{-1}, 2841 cm^{-1} (ν C-H) and 1739 cm^{-1} (ν C=O) were further confirm the synthesis of $(N_3)_7$-βCD-$(PCL)_{14}$. As illustrated in Figure 1(D), the proton signal peaks belonging to the repeating PCL units were located at 4.1-3.8 ppm (-COOCH_2CH_2-), 3.6 ppm (-CH_2CH_2OH), 2.4-2.2 ppm (-CH_2CH_2COO-) and 1.17-1.12 ppm (-COOCH_2CH_2CH_2CH_2CH_2-). Furthermore, the degree of polymerization (DP) of $(N_3)_7$-βCD-$(PCL)_{14}$ was approximately 23, which was calculated by comparing the integration area attributed to protons of the PCL between 4.1-3.8 ppm (-COOCH_2CH_2-) to the signals that appeared at 3.65 ppm (-COOCH_2CH_2CH_2CH_2CH_2OH). From the above results, we could confirm that the 14-arm $(N_3)_7$-βCD-$(PCL)_{14}$ polymer was successfully synthesized.

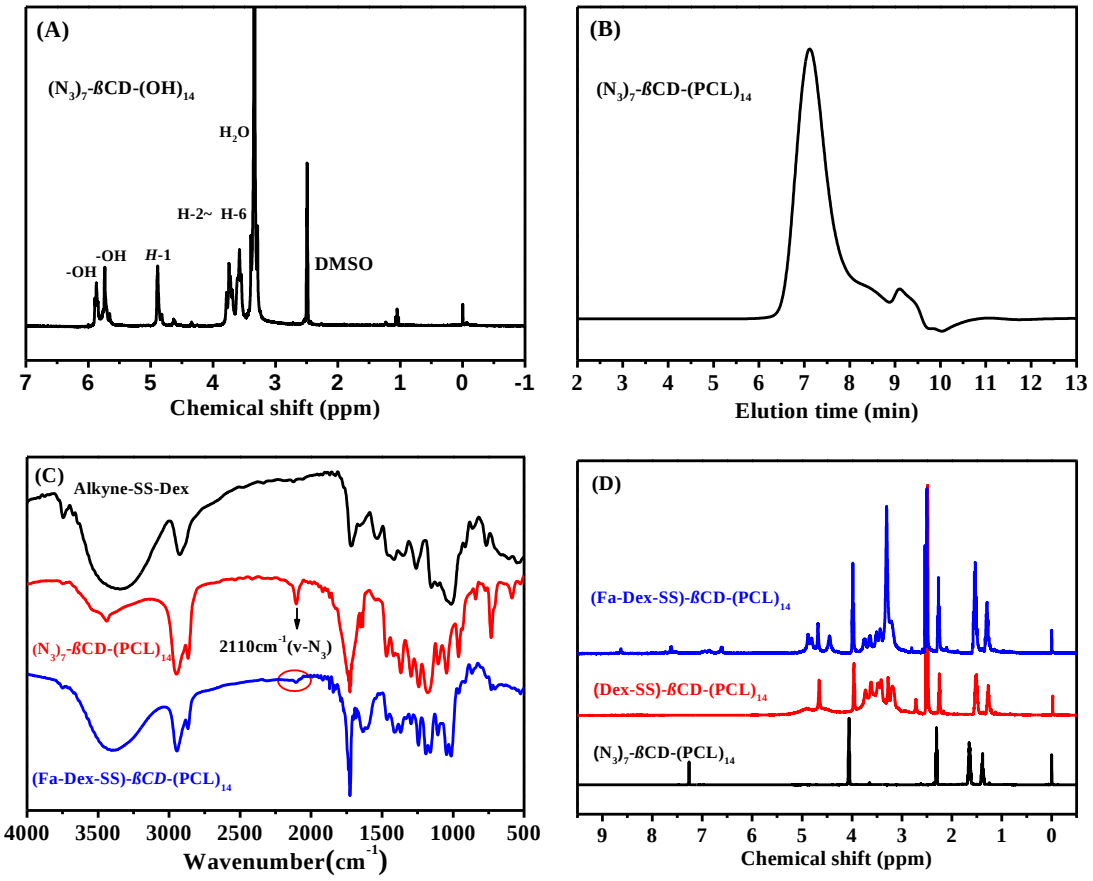

Figure 1 (A) ^{1}H-NMR spectrum for $(N_3)_7$-βCD-$(OH)_{14}$ in DMSO-d6, (B) THF GPC traces obtained for $(N_3)_7$-βCD-$(PCL)_{14}$, (C) FTIR spectra for Alkyne-SS-Dex, $(N_3)_7$-βCD-$(PCL)_{14}$ and (FA-Dex-SS)-βCD-$(PCL)_{14}$, (D) ^{1}H-NMR spectra for $(N_3)_7$-βCD-$(PCL)_{14}$ in $CDCl_3$, (Dex-SS)-βCD-$(PCL)_{14}$ in DMSO-*d*6 and (FA-Dex-SS)-βCD-$(PCL)_{14}$ in DMSO-*d*6.

Preprints (www.preprints.org) | NOT PEER-REVIEWED | Posted: 13 October 2021 doi:10.20944/preprints202110.0196.v1

Many functional groups, such as alkyne or azide groups, can be introduced onto the reducing end of polysaccharides through a reductive amination reaction. Herein, α-alkyne-SS-dextran was synthesized using a procedure similar to that reported by Lecommandoux for the preparation of α-alkyne-dextran reported [41]. From the ^{1}H NMR analysis, we found that the proton peaks belonging to the reducing end group anomeric proton (α-centred at 6.7 ppm and *β*-centred at 6.3 ppm) entirely disappeared, which signified compelling evidence of quantitative reaction.

The click reaction has been widely used to prepare *β*-cyclodextrin-based well-defined star polymer. Alkynyl terminally functionalized linear polymers such as PCL, PNIPAM, dendron-like PAMAM or alkyne-terminated *β*CD precursors could be efficiently grafted-onto the heptakis (6-deoxy-6-azido)-*β*-cyclodextrin via click chemistry[35, 40, 44-46]. Herein, a grafting-onto strategy was applied to synthesize *β*-cyclodextrin-based poly(ε-caprolactone)/dextran star polymer between $(N_3)_7$-*β*CD-$(PCL)_{14}$ and α-alkyne-SS-dextran in DMSO solution at 60 °C for 48 h in the presence of CuBr/PMDETA. In order to synthesize a well-defined (Dex-SS)-*β*CD-$(PCL)_{14}$ star polymer, the molar ratio of α-alkyne-SS-dextran to $(N_3)_7$-*β*CD-$(PCL)_{14}$ was 10: 1. After click chemistry, excess α-alkyne-SS-dextran precursor was facilely removed via dialysis against deionized water for 3 days in a dialysis tube (MWCO 30000 Da). From the ^{1}H NMR spectrum of (Dex-SS)-*β*CD-$(PCL)_{14}$ (Figure 1 (D)), the signals at 4.1-3.8, 3.6, 2.4-2.2 and 1.17-1.12 ppm were due to the methylene protons of the PCL arms, and the dextran proton signals were located at 3.1-4.0 (m, dextran glucosidic protons), 4.7 (s, dextran anomeric proton), 4.5, 4.9, and 5.1 ppm (s, dextran hydroxyl protons), indicating the formation of (Dex-SS)-*β*CD-$(PCL)_{14}$ star polymer. However, as Figure 1 (D) indicated that a weak azide group characteristic absorption peak still observed at 2094 cm^{-1} in FTIR spectrum for the (Dex-SS)-*β*CD-$(PCL)_{14}$, 4/5000. The aforementioned result confirmed that some azide groups remained, even though the α-alkyne-SS-dextran/$(N_3)_7$-*β*CD-$(PCL)_{14}$ molar feed ratio = 10: 1. A similar result was reported by Ai et al, who tried to graft α-alkyne-dextran onto $(N_3)_7$-*β*CD, and found that the steric hindrance of dextran could directly limit the coupling efficiency. Even when

Preprints (www.preprints.org) | NOT PEER-REVIEWED | Posted: 13 October 2021 doi:10.20944/preprints202110.0196.v1

the alkyne/azide molar ration reached up to 14:1, more than two azide groups remained unreacted[39].

(FA-Dex-SS)-βCD-$(PCL)_{14}$ star polymer was prepared via an esterification reaction between the γ-carboxylic acid group of FA and hydroxyl group of dextran[47]. The chemical structure of the targeting compound was confirmed by ^{1}H NMR. As demonstrated in Figure 1(D), by comparison with the ^{1}H NMR spectrum of (Dex-SS)-βCD-$(PCL)_{14}$, we find that three new proton signal peaks appeared d at 6.8, 7.7 and 8.6 ppm, which were attributed to the aromatic proton signals of folic acid. Moreover, the degree of substitution (DS) of FA in (FA-Dex-SS)-βCD-$(PCL)_{14}$ was determined to be 11 wt% (approximately 1.7 FA molecules per dextran), according to the proton peak integrations of the aromatic of FA and dextran protons between 3.2 and 4.0 ppm[47].

3.2 Preparation and characterization of nanoparticles

The (FA-Dex-SS)-βCD-$(PCL)_{14}$ star polymer is composed of hydrophilic dextran arms and hydrophobic PCL arms, therefore, this amphiphilic star polymer can form aggregates in aqueous medium. The critical micelle concentration (CMC) value is an important parameter which was detected by fluorescence of pyrene to describe the formation of aggregates [48]. Figure 2(A) showed the fluorescence excitation spectra of pyrene in (FA-Dex-SS)-βCD-$(PCL)_{14}$ aqueous solutions at various concentrations. At lower concentrations, the fluorescence intensity of pyrene was weak, and the peak nearly unchanged at 335 nm, indicating that pyrene was still in a polar environment. As the star polymer concentrations increased, the fluorescence intensity of pyrene dramatically increased, and an obvious redshift of the excitation peak was observed. It has been reported that pyrene tends to show strong fluorescence intensity when it is encapsulated into hydrophobic microdomains, hence, fluorescence excitation spectra confirmed that pyrene was incorporated into the hydrophobic inner of the nanoparticles. By calculating the ratios of pyrene fluorescence intensities pyrene (I_{337}/ I_{333}) and the concentration of (Fa-Dex-SS)-βCD-$(PCL)_{14}$, the CMC value was approximately 0.0033 mg/mL.

(FA-Dex-SS)-βCD-$(PCL)_{14}$-based blank or drug loaded nanoparticles were

 doi:10.20944/preprints202110.0196.v1

prepared by using the nanoprecipitation method, the particle size and morphology of these nanoparticles were measured by DLS and TEM at a constant concentration of 1 mg/mL. Particle size and distribution were recorded at a constant scattering angle of 90°. As shown in Figure 2(C), a monodispersed size distribution was found, the particle size of the blank nanoparticles was approximately 65 nm, and the polydispersity index was 0.12 in aqueous solution. The morphology of the blank nanoparticles is illustrated in Figure 2(E), TEM imaging showed formation of well-defined spherical particles. It should be noticed that the particle size of the blank nanoparticles measured by DLS is larger than found from the TEM results, which was attributed to the fact that DLS results were recorded in aqueous solution, while TEM images are obtained in the dried state.

As illustrated in Figure 2(D) and Table1, the particle size of the theranostic nanoparticles measured by DLS was larger than blank nanoparticles. The increase in particle size could be attributed to the encapsulation of hydrophobic DOX and the MR contrasting agent SPIO into the hydrophobic microdomains of the (FA-Dex-SS)-βCD-$(PCL)_{14}$ nanoparticles[23]. These SPIO theranostic nanoparticles were well-defined spheroid as shown in Figure 2(F) which observed by TEM. In addition, the DLC and SLC of the star-like polymeric nanoparticles are shown in Table 1. All the nanoparticles exhibited high DOX and SPIO encapsulation capacity.

Preprints (www.preprints.org) | NOT PEER-REVIEWED | Posted: 13 October 2021 doi:10.20944/preprints202110.0196.v1

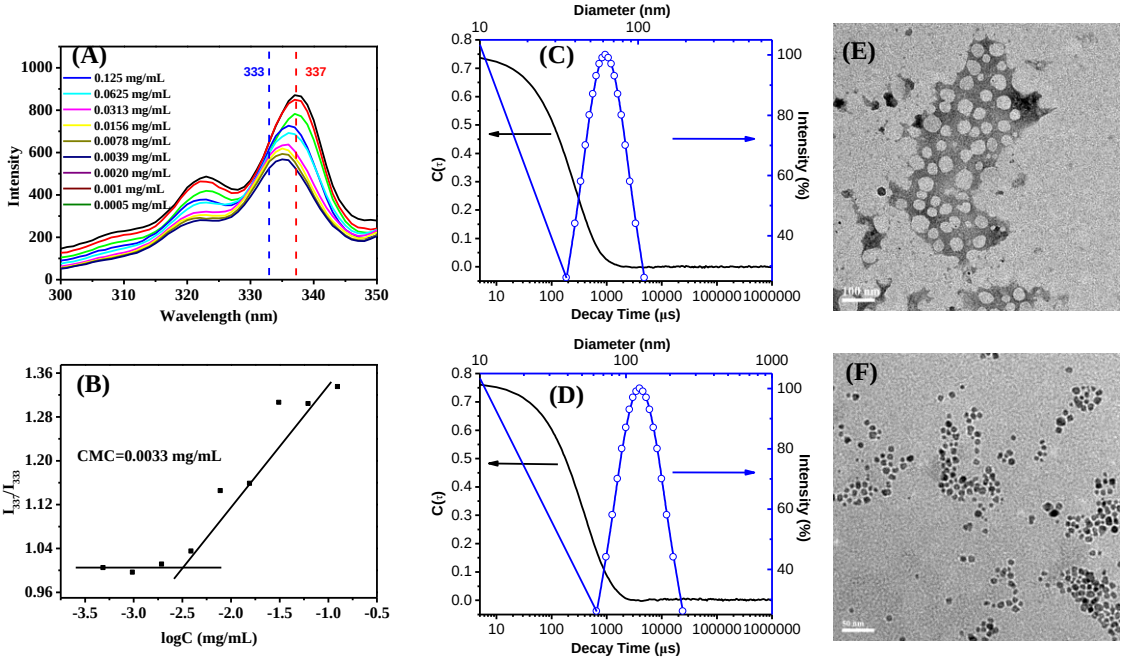

Figure 2 (A) Excitation spectrum for pyrene in (FA-Dex-SS)-βCD-$(PCL)_{14}$ aqueous solutions, (B) Plots of fluorescence intensity ratio I_{337}/I_{333} from pyrene excitation spectra vs log concentration of (FA-Dex-SS)-βCD-$(PCL)_{14}$, (C)Autocorrelation function (C(τ)) and size distribution for blank (FA-Dex-SS)-βCD-$(PCL)_{14}$ solution (1 mg/mL) at 90° and 20 °C, (D) Autocorrelation function (C(τ)) and size distribution for DOX/SPIO loading (FA-Dex-SS)-βCD-$(PCL)_{14}$ solution (1 mg/mL) at 90° and 20 °C, (E) TEM micrography of blank (FA-Dex-SS)-βCD-$(PCL)_{14}$ nanoparticles and (F) TEM micrography of DOX/SPIO loading (FA-Dex-SS)-βCD-$(PCL)_{14}$ nanoparticles.

Table 1 Characteristics of blank and DOX/SPIO-loaded nanoparticles.

Sample code	Blank nanoparticles	DOX/SPIO-loaded nanoparticles		
	Diameter[a]	Diameter(nm)[a]	DLC(%)	SLC(%)
(FA-Dex-SS)-βCD-$(PCL)_{14}$	65.8±2.3	126.8±2.3	11.7	10.3
(FA-Dex)-βCD-$(PCL)_{14}$	77.8±2.3	124.4±1.7	11.2	10.5
(Dex-SS)-βCD-$(PCL)_{14}$	72.3±1.5	127.8±3.7	10.3	10.1
(Dex)-βCD-$(PCL)_{14}$	86.7±3.5	155.8±1.9	10.8	9.8

All aggregate solutions had a final polymer concentration of 0.50 mg/mL. *a* Measured by dynamic light scattering (DLS). b Determined by pyrene-based fluorescent spectrometry.

Preprints (www.preprints.org) | NOT PEER-REVIEWED | Posted: 13 October 2021 doi:10.20944/preprints202110.0196.v1

3.3 Reduction triggered drug release

Reduction-sensitive drug delivery systems can release drugs faster in a highly reductive tumor microenvironment, where the disulfide bond can be cleaved in the presence of GSH. For instance, Zhong et al. prepared disulfide bond-linked dextran-SS-PCL liner block polymers and applied them for the reduction-triggered release of DOX[49]. Herein, the DOX release behaviour from the star polymer nanoparticles was studied in PBS with different GSH concentrations (0 mM, 10 mM) at 37 °C. Figure 3 shows the cumulative release percentages of DOX loaded in the star polymer nanoparticles versus time. In the case of 0 mM GSH, analogous to normal physiological conditions, the release of DOX from the star polymer nanoparticles was slow, and approximately 46.74, 43.86, 40.89 and 43.86 % of the loaded DOX was released from (FA-Dex-SS)-βCD-$(PCL)_{14}$, (FA-Dex)-βCD-$(PCL)_{14}$, (Dex-SS)-βCD-$(PCL)_{14}$ and (Dex)-βCD-$(PCL)_{14}$ nanoparticles within 24 h. In the case of 10 mM GSH, only approximately 47.31 and 49.8% of DOX was released from DOX loaded (FA-Dex)-βCD-$(PCL)_{14}$ and (Dex)-βCD-$(PCL)_{14}$ nanoparticles within 24 h. These results indicated that the presence of GSH has no effect on the release of DOX from reduction-insensitive nanoparticles, and the release of DOX was sustained. However, fast release of DOX was observed from the disulfide bond-linked (FA-Dex-SS)-βCD-$(PCL)_{14}$ and (Dex-SS)-βCD-$(PCL)_{14}$ nanoparticles in the case of 10 mM GSH, which mimicked the intracellular environment, and the DOX cumulative release reached nearly 70% within the first 5 h and approximately 100% within 24 h. Similarly, Park et al. found that CPT was completely released from reduction-sensitive nanoparticles within 20 h, which was caused by cleavage of the disulfide bond in the PEG-SS-PBLG copolymer[28]. The DOX rapidly released from the disulfide bonds-linked nanoparticles in this experiment could ascribe to the cleavage of the disulfide bonds by GSH[10, 27].

Preprints (www.preprints.org) | NOT PEER-REVIEWED | Posted: 13 October 2021 doi:10.20944/preprints202110.0196.v1

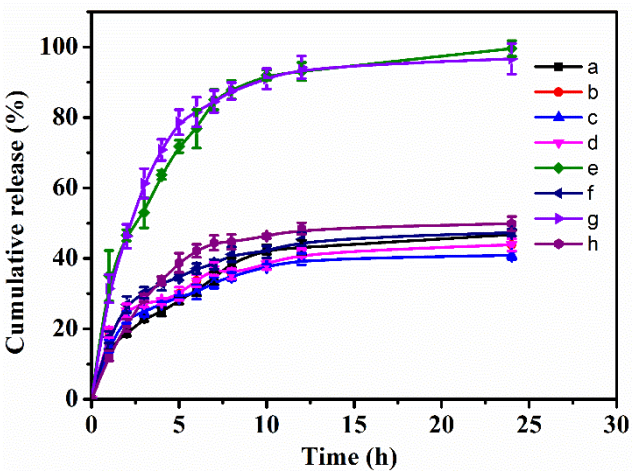

Figure 3 *In vitro* release of DOX from (a) (FA-Dex-SS)-*β*CD-$(PCL)_{14}$, (b) (FA-Dex)-*β*CD-$(PCL)_{14}$, (c) (Dex-SS)-*β*CD-$(PCL)_{14}$ and (d) (Dex)-*β*CD-$(PCL)_{14}$ nanoparticles incubated without GSH; DOX release from DOX-loaded (e) (FA-Dex-SS)-*β*CD-$(PCL)_{14}$, (f) (FA-Dex)-*β*CD-$(PCL)_{14}$, (g) (Dex-SS)-*β*CD-$(PCL)_{14}$ and (h) (Dex)-*β*CD-$(PCL)_{14}$ nanoparticles incubated with 10 mM GSH. The data were presented as mean ± SD (n = 3)

3.4 *In vitro* cell cellular uptake and cytotoxicity

It is well known that the anticancer effects of DOX are due to DOX bounding to chromosomal DNA, leading to cell death[50, 51]. Therefore, the internalization and subcellular distribution of DOX play an important role in the anticancer effects. Herein, CLSM was performed to evaluate the effects of FA and disulfide bonds on the cellular uptake behaviour and intracellular distribution of DOX in folate receptor (FR) positive HepG2 cells. CLSM images figure 4A shown that HepG2 cells treated with free DOX exhibited stronger intracellular DOX fluorescence intensity than cells incubated with DOX/SPIO co-loaded star polymeric nanoparticles in 4 h, whereas, free DOX accumulated in the nucleus predominately. This result can be attributed to the DOX concentration gradient in which DOX passively diffused into the cytosol and was then taken into the nucleus to intercalate into chromosomal DNA[52]. In comparison, the intracellular DOX fluorescence of HepG2 cells incubated with (Dex)-βCD-(PCL)14@DOX/SPIO nanoparticles notably present in the cytoplasm, with almost no

Preprints (www.preprints.org) | NOT PEER-REVIEWED | Posted: 13 October 2021 doi:10.20944/preprints202110.0196.v1

fluorescence in the nucleus, while DOX fluorescence of (Dex-SS)-βCD-(PCL)14@DOX/SPIO nanoparticles was prominently accumulated in the cytosol and substantially less accumulated in the nuclei. This consequence could be attributed to the accelerated DOX release from the nanoparticles under reducing conditions, then DOX diffusing into the nuclei[49]. In HepG2 cells, incubated with the FA-decorated (FA-Dex)-*β*CD-$(PCL)_{14}$@DOX/SPIO nanoparticles, strong DOX fluorescence accumulated in the cytosol, and weak fluorescence accumulated in the nuclei. This result could be associated with folate receptor-mediated endocytosis mechanism. Gong and co-workers found that FA-conjugated SPIO/DOX-loaded vesicles treated HeLa cells showed higher DOX fluorescence than cells treated with FA-free vesicles[53]. Notably, strong DOX fluorescence was observed in the cytoplasm and the nuclei when HepG2 cells were incubated with FA-conjugated reduction-sensitive nanoparticles (FA-Dex-SS)-*β*CD-$(PCL)_{14}$@DOX/SPIO 4 h. These results not only demonstrated that DOX could be efficiently transported into the cytoplasm but also suggested that DOX was rapidly released from the nanoparticles diffused into the cell nuclei when under reducing conditions.

Flow cytometric analysis was performed to further quantify intracellular DOX uptake by HepG2 cells. The fluorescence intensity of DOX in HepG2 cells was quantitatively assayed after free DOX or DOX/SPIO-loaded star polymeric nanoparticles at a DOX concentration of 5 μg/mL cultured for 4 h. As illustrated in Figure 4(B), cells cultured with free DOX showed higher fluorescence intensity owing to a diffusion mechanism of DOX cellular uptake, while DOX/SPIO-loaded star polymeric nanoparticles cultured cells shower lower fluorescence intensity dependent on endocytosis. Flow cytometric analysis demonstrated that the cells treated with nanopartilces decorated with a FA targeting ligand or with a disulfide bonds linkage exhibited higher DOX fluorescence intensity than FA- and disulfide bond-free nanoparticles. The above results confirmed that the folate receptor-mediated endocytosis process or reduction-responsive drug release behaviour can enhance the intracellular DOX fluorescence intensity. Furthermore, we wondered whether the

Preprints (www.preprints.org) | NOT PEER-REVIEWED | Posted: 13 October 2021 doi:10.20944/preprints202110.0196.v1

introduction of folic acid and disulfide bonds contemporary could more efficiently enhance intracellular DOX uptake. To confirm this, the FA-targeting ligands and disulfide bond star polymer (FA-Dex-SS)-βCD-(PCL)14@DOX/SPIO was developed as a theranostic nanoparticle for tumor treatment and diagnosis. As anticipated, cells which were treated with (FA-Dex-SS)-βCD-(PCL)14@DOX/SPIO nanoparticles exhibited the strongest intracellular fluorescence of DOX among all these cells treated by star polymeric nanoparticles, which suggest cellular uptake these nanoparticles rapidly and their release DOX speedily from nanoparticles. These results imply that the (FA-Dex-SS)-βCD-$(PCL)_{14}$ polymer is a promising nano-cargo for tumor-targeted drug delivery, which has conformance with the CLSM observations.

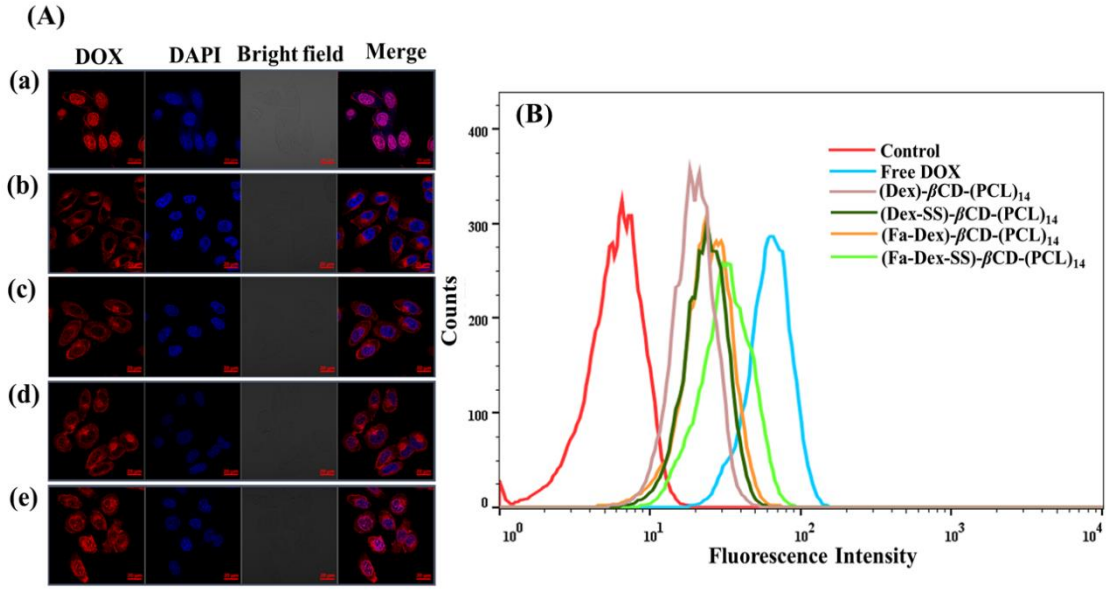

Figure 4. *In vitro* cell cellular uptake analysis by (A) CLSM after HepG2 cells incubated with (a) Free DOX, (b) (Dex)-βCD-$(PCL)_{14}$@DOX/SPIO, (c) (Dex-SS)-βCD-$(PCL)_{14}$@DOX/SPIO, (d) (FA-Dex)-βCD-$(PCL)_{14}$@DOX/SPIO and (e) (FA-Dex-SS)-βCD-$(PCL)_{14}$@DOX/SPIO at 5 μg/mL DOX for 4 h. (B) DOX fluorescence intensity of HepG2 cells incubated with free DOX and DOX/SPIO-loaded polymeric nanoparticles at 5 μg/mL DOX for 4 h measured by flow cytometry.

In vitro cellular uptake effects of the star polymeric nanoparticles were demonstrated by Prussian blue staining. As shown in Figure 5, blue spots appeared

Preprints (www.preprints.org) | NOT PEER-REVIEWED | Posted: 13 October 2021 doi:10.20944/preprints202110.0196.v1

when HepG2 cells were treated with DOX/SPIO-loaded star polymeric nanoparticles for 3 h. Similar to the CLSM and flow cytometric results, the cells incubated with (FA-Dex-SS)-βCD-$(PCL)_{14}$@DOX/SPIO nanoparticles showed more blue spots than their counterparts.

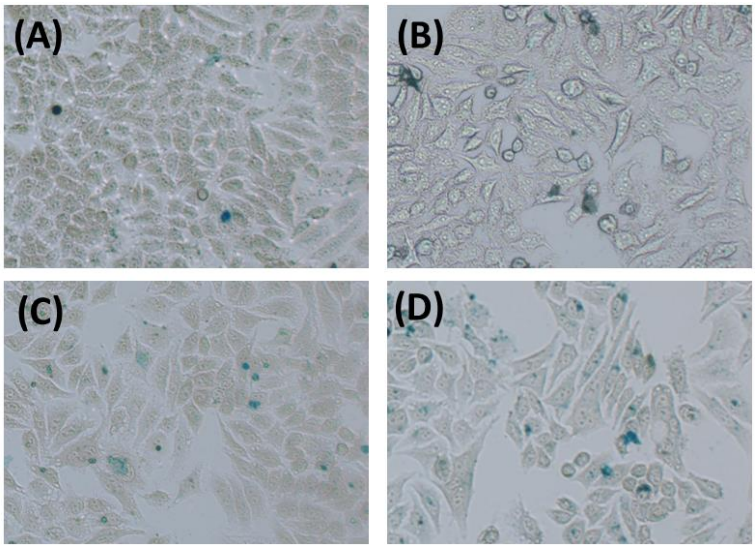

Figure 5 Prussian blue staining images of HepG2 cells incubated with (A) (Dex)-βCD-$(PCL)_{14}$@DOX/SPIO, (B) (Dex-SS)-βCD-$(PCL)_{14}$@DOX/SPIO, (C) (FA-Dex)-βCD-$(PCL)_{14}$@DOX/SPIO and (D) (FA-Dex-SS)-βCD-$(PCL)_{14}$@DOX/SPIO at 5 μg/mL SPIO for 4 h.

MTT assay was applied to evaluate *in vitro* cytotoxicity of free DOX and DOX/SPIO-loaded βCD base star polymeric nanoparticles towards HepG2 cells. MTT assay results in Figure 6 showed, cell growth inhibition was limited by DOX concentrations and incubation time. Normally, free DOX exhibits higher cytotoxicity to HepG2 cells than DOX/SPIO-loaded star polymeric nanoparticles, due to free DOX transported into cells through a passive diffusion mechanism. Notably, after 48 h of incubation, the FA-conjugated ((FA-Dex)-βCD-$(PCL)_{14}$) or reduction sensitive ((Dex-SS)-βCD-$(PCL)_{14}$) DOX/SPIO-loaded polymeric nanoparticles showed higher cytotoxicity than the polymeric nanoparticles without targeting molecules or disulfide bonds. It's worth paying more attention to the efficacy of tumor cell growth inhibition for (FA-Dex-SS)-βCD-$(PCL)_{14}$@DOX/SPIO nanoparticles, which was markedly

Preprints (www.preprints.org) | NOT PEER-REVIEWED | Posted: 13 October 2021 doi:10.20944/preprints202110.0196.v1

enhanced compared to (Dex)-βCD-$(PCL)_{14}$@DOX/SPIO and (Dex-SS)-βCD-$(PCL)_{14}$@DOX/SPIO nanoparticles. This phenomenon was probably caused by folate receptor-mediated internalization and cleavage of the disulfide bonds in the reducing environment.

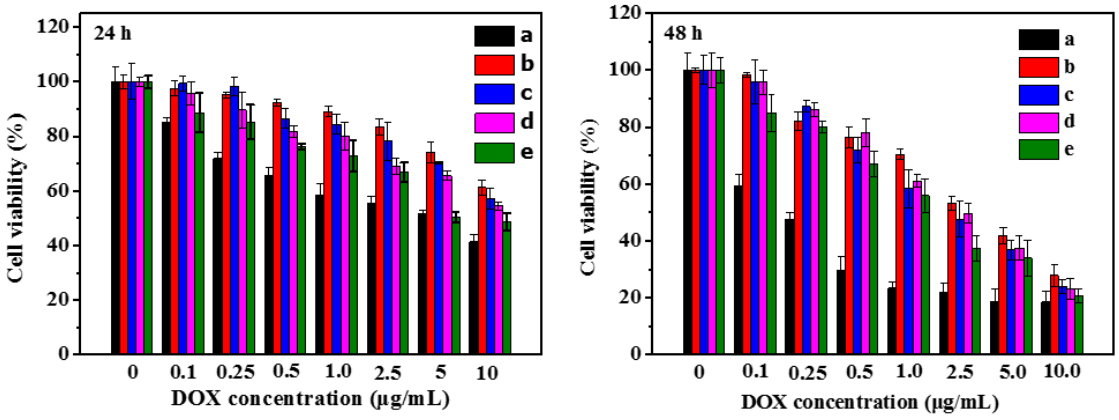

Figure 6 *In vitro* cell cytotoxicity of HepG2 cells incubated with (a) Free DOX, (b) (Dex)-βCD-$(PCL)_{14}$@ DOX/SPIO, (c) (Dex-SS)-βCD-$(PCL)_{14}$@ DOX/SPIO, (d) (FA-Dex)-βCD-$(PCL)_{14}$@ DOX/SPIO and (e) (FA-Dex-SS)-βCD-$(PCL)_{14}$@ DOX/SPIO for 24 and 48 h. The error bars in the graph represent standard deviations (n= 3).

Quantitative determination of the apoptotic and necrotic activities of free DOX and DOX/SPIO-loaded polymeric nanoparticles towards HepG2 cells was further investigated by Annexin V-FITC and DAPI flow cytometric assays at a DOX dose of 5 μg/mL. As illustrated in Figure 6, cells incubated in pure culture medium for 24 h showed very low apoptotic activity. HepG2 cells treated with free DOX demonstrated the strongest effect on cell apoptosis (46.79%) among all the test groups, which was attributed to the passive diffusion cellular uptake mechanisms. As a reduction-insensitive nanocarrier without targeting capacity, the ratio of apoptotic cells in the (Dex)-βCD-$(PCL)_{14}$@DOX/SPIO group was approximately 19.07%. In comparison, DOX delivered by reduction-sensitive (Dex-SS)-βCD-$(PCL)_{14}$ polymeric nanoparticles resulted in 25.99% cell apoptosis. A better apoptosis effect resulted from the cells incubated with FA-decorated (FA-Dex)-βCD-$(PCL)_{14}$@DOX/SPIO nanoparticles, leading to 30.88% apoptotic cells. As expected, cells treated with (FA-Dex-SS)-βCD-

Preprints (www.preprints.org) | NOT PEER-REVIEWED | Posted: 13 October 2021 doi:10.20944/preprints202110.0196.v1

(PCL)14@DOX/SPIO polymeric nanoparticles performed excellently on leading cells apoptotic which percentage of apoptotic cells up to 36.72%. The above results demonstrated that the *β*-cyclodextrin-based poly(ε-caprolactone)/dextran star polymer with FA conjugattion and reduction-triggered properties showed promising potential as a tumor-targeted drug nanocarrier.

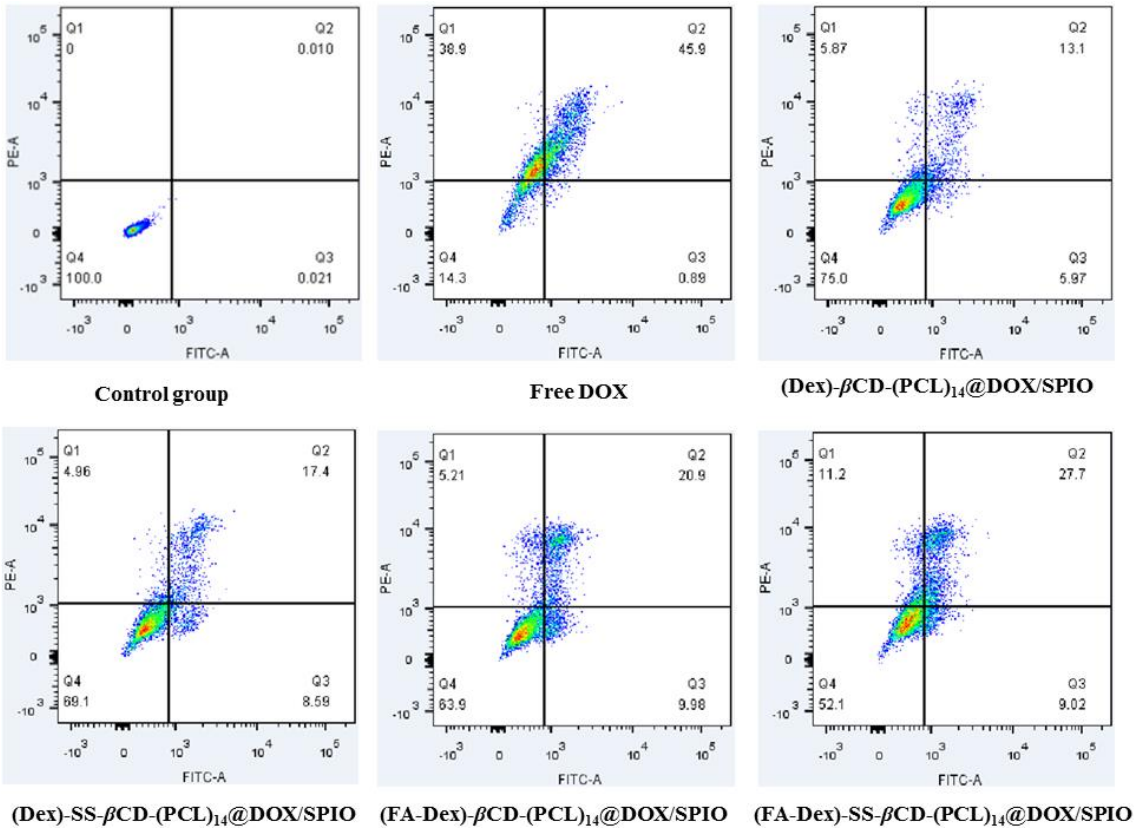

Figure 7 Cells apoptosis analysis by flow cytometry after HepG2 cells incubated with free DOX and DOX loaded nanoparticles at 5 μg/mL DOX for 24 h.

3.6 MRI contrast measurement

Currently, the development of SPIO-based theranostic nanoparticles has attracted considerable attention, and SPIO-based MRI contrast agents can dramatically shorten the T_2 (spin-spin) relaxation times[54]. T_2 relaxivity can be calculated from the linear relationship of 1/relaxation time (s^{-1}) versus iron concentrations (mM Fe). In this work, the T_2 relaxation rate of (FA-Dex-SS)-*β*CD-$(PCL)_{14}$@DOX/SPIO nanoparticles was measured in a 3.0 T field strength clinical MRI scanner. Figure 8(A) shows the T_2 rates of the SPIO-loaded nanoparticles versus iron concentrations, and the transverse

Preprints (www.preprints.org) | NOT PEER-REVIEWED | Posted: 13 October 2021 doi:10.20944/preprints202110.0196.v1

relaxation time calculated from the T_2 rate of the iron concentration was approximately 250.1 Fe $mM^{-1}s^{-1}$, indicating an improved relaxation property. It has been reported that SPIO nanoparticles can be loaded into the compact inner core of nanoparticles, which can shorten the distance of each SPIO and favour magnetic coupling between the SPIO, increasing r_2[39, 55]. The negative contrast enhancement ability of (FA-Dex-SS)-βCD-$(PCL)_{14}$@DOX/SPIO nanoparticles was evaluated from the T_2-weighted images in Figure 8(B). As the T_2-weighted images illustrated, as the iron concentration increased, the signals darkened dramatically.

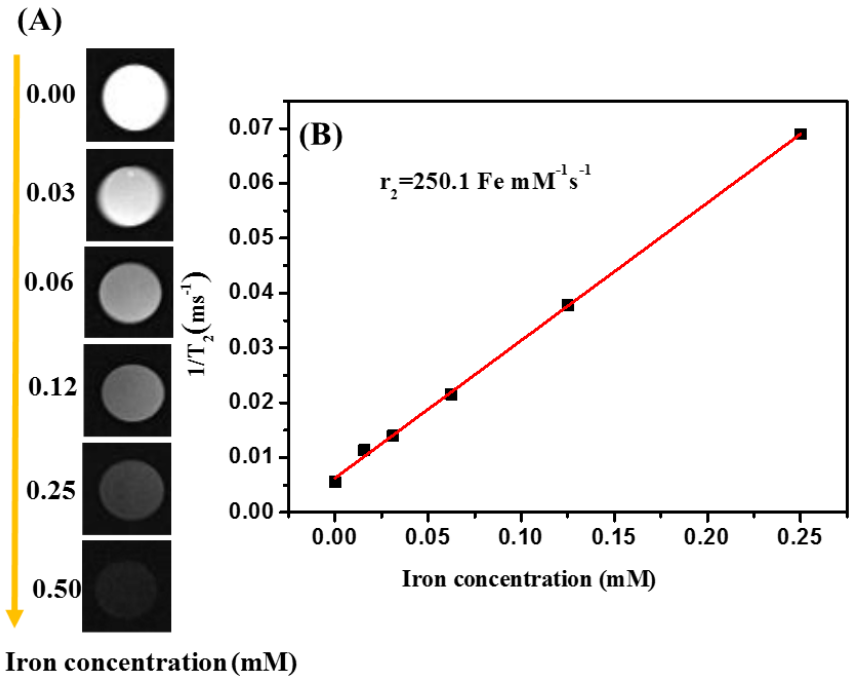

Figure 8 (A) T_2 relaxation rate and (B) T_2-mapping images of (FA-Dex-SS)-βCD-$(PCL)_{14}$@DOX/SPIO nanoparticles at various Fe concentrations (mM).

4. Conclusions

In this study, a folic acid-decorated β-cyclodextrin-based poly(ε-caprolactone)/dextran star polymer was successfully synthesized via the ring opening polymerization combined with Cu(I) catalyed click chemistry and performed as a theranostic nanoparticle for tumor-targeted MRI and chemotherapy. The chemical characteristics of the star polymer were confirmed by GPC, FTIR and ^{1}H NMR analyses. Due to the amphiphilic features of star polymer that could self-assemble into spherical

 doi:10.20944/preprints202110.0196.v1

nanoparticles with an average size of approximately 70 nm. Theranostic nanoparticles were obtained after loading DOX and SPIO inside the core of these nanoparticles. *In vitro* drug release experiments confirmed that disulfide bond-linked theranostic nanoparticles rapidly released DOX in the presence of a high GSH concentration. *In vitro* cellular uptake and cytotoxicity assays suggested that FA-decorated reduction-sensitive nanoparticles exhibited higher intracellular uptake and a greater proliferation inhibitory effect than their counterparts. Moreover, after loading SPIO inside the compact core of the nanoparticles, the T_2 relaxation rate increased to 250.1 Fe $mM^{-1}s^{-1}$. Therefore, FA-decorated reduction-sensitive star polymeric nanoparticles show great potential as theranostic nanocarriers for tumor-targeted drug delivery and diagnosis applications.

Acknowledgement

This work was supported by the National Natural Science Foundation of China (81571665, 81971574), the Science Foundation of Guangzhou First People's Hospital (M2019017), Guangdong Medical Science and Research Foundation (A2019071), Guangzhou General Science and Technology Project of Health and Family Planning (20191A011012), the Science and Technology Project of Guangzhou (201904010422, 202002030268, 202102010025, 202102080158), the Natural Science Foundation of Guangdong Province in China (2021A1515011350, 2018A030313282), the Special Fund for the Construction of High-level Key Clinical Specialty (Medical Imaging) in Guangzhou and Guangzhou Key Laboratory of Molecular Imaging and Clinical Translational Medicine

References

1. Zhou, L.; Wang, H.; Li, Y., Stimuli-Responsive Nanomedicines for Overcoming Cancer Multidrug Resistance. *Theranostics* **2018,** 8, (4), 1059-1074.
2. Fan, C. H.; Cheng, Y. H.; Ting, C. Y.; Ho, Y. J.; Hsu, P. H.; Liu, H. L.; Yeh, C. K., Ultrasound/Magnetic Targeting with SPIO-DOX-Microbubble Complex for Image-Guided Drug Delivery in Brain Tumors. *Theranostics* **2016,** 6, (10), 1542-56.
3. Yilmaz, G.; Demir, B.; Timur, S.; Becer, C. R., Poly(methacrylic acid)-Coated Gold Nanoparticles: Functional Platforms for Theranostic Applications. *Biomacromolecules* **2016,** 17, (9), 2901-11.
4. Janib, S. M.; Moses, A. S.; MacKay, J. A., Imaging and drug delivery using theranostic nanoparticles. *Adv Drug Deliv Rev* **2010,** 62, (11), 1052-1063.
5. Hu, M.; Shen, Y.; Zhang, L.; Qiu, L., Polymersomes via Self-Assembly of Amphiphilic β-Cyclodextrin-Centered Triarm Star Polymers for Enhanced Oral Bioavailability of Water-Soluble Chemotherapeutics. *Biomacromolecules* **2016,** 17, (3), 1026-39.
6. De Beer, E. L.; Bottone, A. E.; Voest, E. E., Doxorubicin and mechanical performance of cardiac trabeculae after acute and chronic treatment: a review. *Eur J Pharmacol* **2001,** 415, (1), 1-11.
7. Kim, J. E.; Cho, H. J.; Kim, J. S.; Shim, C. K.; Chung, S. J.; Oak, M. H.; Yoon, I. S.; Kim, D. D., The limited intestinal absorption via paracellular pathway is responsible for the low oral bioavailability of doxorubicin. *Xenobiotica* **2013,** 43, (7), 579-91.
8. Turakhia, S.; Venkatakrishnan, C. D.; Dunsmore, K.; Wong, H.; Kuppusamy, P.; Zweier, J. L.; Ilangovan, G., Doxorubicin-induced cardiotoxicity: direct correlation of cardiac fibroblast and H9c2 cell survival and aconitase activity with heat shock protein 27. *Am J Physiol Heart Circ Physiol* **2007,** 293, (5), 14.
9. Upadhyay, K. K.; Bhatt, A. N.; Mishra, A. K.; Dwarakanath, B. S.; Jain, S.; Schatz, C.; Le Meins, J. F.; Farooque, A.; Chandraiah, G.; Jain, A. K.; Misra, A.; Lecommandoux, S., The intracellular drug delivery and anti tumor activity of doxorubicin loaded poly(gamma-benzyl L-glutamate)-b-hyaluronan polymersomes. *Biomaterials* **2010,** 31, (10), 2882-92.
10. Yang, H.-K.; Qi, M.; Mo, L.; Yang, R.-M.; Xu, X.-D.; Bao, J.-F.; Tang, W.-J.; Lin, J.-T.; Zhang, L.-M.; Jiang, X.-Q., Reduction-sensitive amphiphilic dextran derivatives as theranostic nanocarriers for chemotherapy and MR imaging. *RSC Advances* **2016,** 6, (115), 114519-114531.
11. Tang, H.; Zhang, J.; Tang, J.; Shen, Y.; Guo, W.; Zhou, M.; Wang, R.; Jiang, N.; Gan, Z.; Yu, Q., Tumor Specific and Renal Excretable Star-like Triblock Polymer-Doxorubicin Conjugates for Safe and Efficient Anticancer Therapy. *Biomacromolecules* **2018,** 19, (7), 2849-2862.
12. Jain, R. K.; Stylianopoulos, T., Delivering nanomedicine to solid tumors. *Nat Rev Clin Oncol* **2010,** 7, (11), 653-64.
13. **!!! INVALID CITATION !!!**
14. Mura, S.; Nicolas, J.; Couvreur, P., Stimuli-responsive nanocarriers for drug delivery. *Nat Mater* **2013,** 12, (11), 991-1003.
15. Sulistio, A.; Lowenthal, J.; Blencowe, A.; Bongiovanni, M. N.; Ong, L.; Gras, S. L.; Zhang, X.; Qiao, G. G., Folic acid conjugated amino acid-based star polymers for active targeting of cancer cells. *Biomacromolecules* **2011,** 12, (10), 3469-77.

16. Yang, H.-K.; Bao, J.-F.; Mo, L.; Yang, R.-M.; Xu, X.-D.; Tang, W.-J.; Lin, J.-T.; Wang, G.-H.; Zhang, L.-M.; Jiang, X.-Q., *Bioreducible amphiphilic block copolymers based on PCL and glycopolypeptide as multifunctional theranostic nanocarriers for drug delivery and MR imaging*. 2017; Vol. 7, p 21093-21106.
17. Katsamakas, S.; Chatzisideri, T.; Thysiadis, S.; Sarli, V., RGD-mediated delivery of small-molecule drugs. *Future Med Chem* **2017,** 9, (6), 579-604.
18. Qian, Z. M.; Li, H.; Sun, H.; Ho, K., Targeted drug delivery via the transferrin receptor-mediated endocytosis pathway. *Pharmacol Rev* **2002,** 54, (4), 561-87.
19. Mould, D. R.; Meibohm, B., Drug Development of Therapeutic Monoclonal Antibodies. *BioDrugs* **2016,** 30, (4), 275-93.
20. Zhao, F.; Yin, H.; Zhang, Z.; Li, J., Folic acid modified cationic γ-cyclodextrin-oligoethylenimine star polymer with bioreducible disulfide linker for efficient targeted gene delivery. *Biomacromolecules* **2013,** 14, (2), 476-84.
21. Weitman, S. D.; Lark, R. H.; Coney, L. R.; Fort, D. W.; Frasca, V.; Zurawski, V. R., Jr.; Kamen, B. A., Distribution of the folate receptor GP38 in normal and malignant cell lines and tissues. *Cancer Res* **1992,** 52, (12), 3396-401.
22. Canal, F.; Vicent, M. J.; Pasut, G.; Schiavon, O., Relevance of folic acid/polymer ratio in targeted PEG-epirubicin conjugates. *J Control Release* **2010,** 146, (3), 388-99.
23. Yang, X.; Chen, Y.; Yuan, R.; Chen, G.; Blanco, E.; Gao, J.; Shuai, X., Folate-encoded and Fe3O4-loaded polymeric micelles for dual targeting of cancer cells. *Polymer* **2008,** 49, (16), 3477-3485.
24. Yang, X.; Grailer, J. J.; Rowland, I. J.; Javadi, A.; Hurley, S. A.; Steeber, D. A.; Gong, S., Multifunctional SPIO/DOX-loaded wormlike polymer vesicles for cancer therapy and MR imaging. *Biomaterials* **2010,** 31, (34), 9065-73.
25. Zhou, Q.; Zhang, L.; Yang, T.; Wu, H., Stimuli-responsive polymeric micelles for drug delivery and cancer therapy. *Int J Nanomedicine* **2018,** 13, 2921-2942.
26. Balendiran, G. K.; Dabur, R.; Fraser, D., The role of glutathione in cancer. *Cell Biochem Funct* **2004,** 22, (6), 343-52.
27. Zhang, A.; Zhang, Z.; Shi, F.; Ding, J.; Xiao, C.; Zhuang, X.; He, C.; Chen, L.; Chen, X., Disulfide crosslinked PEGylated starch micelles as efficient intracellular drug delivery platforms. *Soft Matter* **2013,** 9, (7), 2224-2233.
28. Thambi, T.; Yoon, H. Y.; Kim, K.; Kwon, I. C.; Yoo, C. K.; Park, J. H., Bioreducible block copolymers based on poly(ethylene glycol) and poly(γ-benzyl L-glutamate) for intracellular delivery of camptothecin. *Bioconjug Chem* **2011,** 22, (10), 1924-31.
29. England, R. M.; Moss, J. I.; Gunnarsson, A.; Parker, J. S.; Ashford, M. B., Synthesis and Characterization of Dendrimer-Based Polysarcosine Star Polymers: Well-Defined, Versatile Platforms Designed for Drug-Delivery Applications. *Biomacromolecules* **2020,** 21, (8), 3332-3341.
30. Willner, L.; Jucknischke, O.; Richter, D.; Roovers, J.; Zhou, L. L.; Toporowski, P. M.; Fetters, L. J.; Huang, J. S.; Lin, M. Y.; Hadjichristidis, N., Structural Investigation of Star Polymers in Solution by Small-Angle Neutron Scattering. *Macromolecules* **1994,** 27, (14), 3821-3829.
31. Loftsson, T.; Brewster, M. E., Cyclodextrins as functional excipients: methods to enhance complexation efficiency. *J Pharm Sci* **2012,** 101, (9), 3019-32.
32. Liao, R.; Lv, P.; Wang, Q.; Zheng, J.; Feng, B.; Yang, B., Cyclodextrin-based biological

stimuli-responsive carriers for smart and precision medicine. *Biomater Sci* **2017,** 5, (9), 1736-1745.

33. Toomari, Y.; Namazi, H.; Akbar, E. A., Synthesis of the dendritic type β-cyclodextrin on primary face via click reaction applicable as drug nanocarrier. *Carbohydr Polym* **2015,** 132, 205-13.
34. Toomari, Y.; Namazi, H.; Entezami, A. A., Fabrication of biodendrimeric β-cyclodextrin via click reaction with potency of anticancer drug delivery agent. *Int J Biol Macromol* **2015,** 79, 883-93.
35. López-Méndez, L. J.; González-Méndez, I.; Aguayo-Ortiz, R.; Dominguez, L.; Alcaraz-Estrada, S. L.; Rojas-Aguirre, Y.; Guadarrama, P., Synthesis of a poly(ester) dendritic β-cyclodextrin derivative by "click" chemistry: Combining the best of two worlds for complexation enhancement. *Carbohydr Polym* **2018,** 184, 20-29.
36. Gou, P. F.; Zhu, W. P.; Shen, Z. Q., Synthesis, self-assembly, and drug-loading capacity of well-defined cyclodextrin-centered drug-conjugated amphiphilic A(14)B(7) Miktoarm star copolymers based on poly(epsilon-caprolactone) and poly(ethylene glycol). *Biomacromolecules* **2010,** 11, (4), 934-43.
37. Li, N.; Luo, H. C.; Ren, M.; Zhang, L. M.; Wang, W.; Pan, C. L.; Yang, L. Q.; Lao, G. J.; Deng, J. J.; Mai, K. J.; Sun, K.; Yang, C.; Yan, L., Efficiency and Safety of β-CD-(D(3))(7) as siRNA Carrier for Decreasing Matrix Metalloproteinase-9 Expression and Improving Wound Healing in Diabetic Rats. *ACS Appl Mater Interfaces* **2017,** 9, (20), 17417-17426.
38. Méndez-Ardoy, A.; Guilloteau, N.; Di Giorgio, C.; Vierling, P.; Santoyo-González, F.; Ortiz Mellet, C.; García Fernández, J. M., β-Cyclodextrin-based polycationic amphiphilic "click" clusters: effect of structural modifications in their DNA complexing and delivery properties. *J Org Chem* **2011,** 76, (15), 5882-94.
39. Su, H.; Liu, Y.; Wang, D.; Wu, C.; Xia, C.; Gong, Q.; Song, B.; Ai, H., Amphiphilic starlike dextran wrapped superparamagnetic iron oxide nanoparticle clsuters as effective magnetic resonance imaging probes. *Biomaterials* **2013,** 34, (4), 1193-203.
40. Xu, J.; Liu, S., Synthesis of well-defined 7-arm and 21-arm poly(N-isopropylacrylamide) star polymers with β-cyclodextrin cores via click chemistry and their thermal phase transition behavior in aqueous solution. *Journal of Polymer Science Part A: Polymer Chemistry* **2009,** 47, (2), 404-419.
41. Schatz, C.; Louguet, S.; Le Meins, J.-F.; Lecommandoux, S., Polysaccharide-block-polypeptide Copolymer Vesicles: Towards Synthetic Viral Capsids. *Angewandte Chemie International Edition* **2009,** 48, (14), 2572-2575.
42. Le, H. T.; Jeon, H. M.; Lim, C. W.; Kim, T. W., Synthesis, cytotoxicity, and phase-solubility study of cyclodextrin click clusters. *J Pharm Sci* **2014,** 103, (10), 3183-9.
43. Chang, L.; Deng, L.; Wang, W.; Lv, Z.; Hu, F.; Dong, A.; Zhang, J., Poly(ethyleneglycol)-b-poly(ε-caprolactone-co-γ-hydroxyl-ε- caprolactone) bearing pendant hydroxyl groups as nanocarriers for doxorubicin delivery. *Biomacromolecules* **2012,** 13, (10), 3301-10.
44. Hoogenboom, R.; Moore, B. C.; Schubert, U. S., Synthesis of star-shaped poly(epsilon-caprolactone) via'click' chemistry and 'supramolecular click' chemistry. *Chem Commun* **2006,** 14, (38), 4010-2.
45. Deng, J.; Li, N.; Mai, K.; Yang, C.; Yan, L.; Zhang, L.-M., Star-shaped polymers consisting of a β-cyclodextrin core and poly(amidoamine) dendron arms: binding and release studies

with methotrexate and siRNA. *Journal of Materials Chemistry* **2011,** 21, (14), 5273-5281.

46. Zhang, J.; Ellsworth, K.; Ma, P. X., Synthesis of β-cyclodextrin containing copolymer via "click" chemistry and its self-assembly in the presence of guest compounds. *Macromolecular Rapid Communications* **2012,** 33, (8), 664-671.
47. Tang, Y.; Li, Y.; Xu, R.; Li, S.; Hu, H.; Xiao, C.; Wu, H.; Zhu, L.; Ming, J.; Chu, Z.; Xu, H.; Yang, X.; Li, Z., Self-assembly of folic acid dextran conjugates for cancer chemotherapy. *Nanoscale* **2018,** 10, (36), 17265-17274.
48. Wilhelm, M.; Zhao, C. L.; Wang, Y.; Xu, R.; Winnik, M. A.; Mura, J. L.; Riess, G.; Croucher, M. D., Poly(styrene-ethylene oxide) block copolymer micelle formation in water: a fluorescence probe study. *Macromolecules* **1991,** 24, (5), 1033-1040.
49. Sun, H.; Guo, B.; Li, X.; Cheng, R.; Meng, F.; Liu, H.; Zhong, Z., Shell-sheddable micelles based on dextran-SS-poly(epsilon-caprolactone) diblock copolymer for efficient intracellular release of doxorubicin. *Biomacromolecules* **2010,** 11, (4), 848-54.
50. Zunino, F.; Di Marco, A.; Zaccara, A.; Gambetta, R. A., The interaction of daunorubicin and doxorubicin with DNA and chromatin. *Biochim Biophys Acta* **1980,** 607, (2), 206-14.
51. Zunino, F.; Gambetta, R.; Di Marco, A.; Velcich, A.; Zaccara, A.; Quadrifoglio, F.; Crescenzi, V., The interaction of adriamycin and its beta anomer with DNA. *Biochim Biophys Acta* **1977,** 476, (1), 38-46.
52. Shuai, X.; Ai, H.; Nasongkla, N.; Kim, S.; Gao, J., Micellar carriers based on block copolymers of poly(epsilon-caprolactone) and poly(ethylene glycol) for doxorubicin delivery. *J Control Release* **2004,** 98, (3), 415-26.
53. Yang, X.; Grailer, J. J.; Rowland, I. J.; Javadi, A.; Hurley, S. A.; Matson, V. Z.; Steeber, D. A.; Gong, S., Multifunctional stable and pH-responsive polymer vesicles formed by heterofunctional triblock copolymer for targeted anticancer drug delivery and ultrasensitive MR imaging. *ACS Nano* **2010,** 4, (11), 6805-17.
54. Sanson, C.; Diou, O.; Thévenot, J.; Ibarboure, E.; Soum, A.; Brûlet, A.; Miraux, S.; Thiaudière, E.; Tan, S.; Brisson, A.; Dupuis, V.; Sandre, O.; Lecommandoux, S., Doxorubicin loaded magnetic polymersomes: theranostic nanocarriers for MR imaging and magneto-chemotherapy. *ACS Nano* **2011,** 5, (2), 1122-40.
55. Taktak, S.; Sosnovik, D.; Cima, M. J.; Weissleder, R.; Josephson, L., Multiparameter magnetic relaxation switch assays. *Anal Chem* **2007,** 79, (23), 8863-9.